



PAPER

Designing RNAs with Language Models

Milan Gautam,¹ Ning Dai,¹ Tianshuo Zhou,¹ Bowen Xie,¹ David Mathews³, Liang Huang^{1,*}

¹School of EECS, ²Dept. of Biochemistry & Biophysics, Oregon State University, USA, ³Dept. of Biochemistry & Biophysics, ⁴Center for RNA Biology and ⁵Dept. of Biostatistics and Computational Biology, University of Rochester Medical Center, USA

Abstract

RNA design, the task of finding a sequence that folds into a target secondary structure, has broad biological and biomedical impact but remains computationally challenging due to the exponentially large sequence space and exponentially many competing folds. Traditional approaches treat it as an optimization problem, relying on per-instance heuristics or constraint-based search. We instead reframe RNA design as conditional sequence generation and introduce a reusable neural approximator, instantiated as an autoregressive language model (LM), that maps target structures directly to sequences. We first train our model in a supervised setting on random-induced structure-sequence pairs, and then use reinforcement learning (RL) to optimize end-to-end metrics. We also propose methods to select a small subset for RL that greatly improves RL efficiency and quality. Across four datasets, our approach outperforms state-of-the-art systems on key metrics such as Boltzmann probability while being $1.7\times$ faster, establishing conditional LM generation as a scalable, task-agnostic alternative to per-instance optimization for RNA design. Our code and data are available at <https://github.com/KuNyaa/RNA-Design-LM>.

Key words: RNA design, language model, reinforcement learning

1. Introduction

RNA plays a central role in cellular processes such as transcription, translation, catalysis, and gene regulation (Eddy., 2001; Doudna and Cech, 2002; Bachellerie *et al.*, 2002). Its biological and biomedical importance is underscored by RNA viruses like SARS-CoV-2, as well as the Nobel Prizes in both 2023 (mRNA vaccine) and 2024 (microRNAs). Since structure determines function, designing artificial RNA molecules with specific secondary structures enables a wide range of applications, including artificial ribozymes (Dotu *et al.*, 2014; Yamagami *et al.*, 2018), microRNAs (Schwab *et al.*, 2006), aptamers (Hamada, 2018), and riboswitches (Bauer and Suess, 2006; Findeiß *et al.*, 2017).

The problem of *RNA design*, also known as *RNA inverse folding*, aims to find an RNA sequence that folds into a given target structure (Hofacker *et al.*, 1994; Andronescu *et al.*, 2004; Garcia-Martin *et al.*, 2013; Zadeh *et al.*, 2011b; Zhou *et al.*, 2023). Computationally, this is an exceptionally challenging problem due to two levels of combinatorial explosion, both in the *sequence (design) space* and *structure (folding) space*. For any target structure, there are exponentially many candidate designs, while for each design, there are also exponentially many alternative structures that compete with the target.

Indeed, the problem has been proven NP-hard under simplified energy models (Bonnet *et al.*, 2020).

Existing approaches to RNA design can be broadly categorized into three camps. The most common one is heuristic local search that iteratively mutates candidate sequences, such as RNAinverse (Hofacker *et al.*, 1994), NEMO (Portela, 2018) and SAMFEO (Zhou *et al.*, 2023). Operating on one or a few sequences at a time, they cannot keep up with the exponential growth of the design space and struggle at long and hard-to-design structures. To address this fundamental problem, the second camp recursively decomposes large structures into smaller ones, which includes RNA-SSD (Andronescu *et al.*, 2004), RNAiFold (Garcia-Martin *et al.*, 2013), and NUPACK (Zadeh *et al.*, 2011b). Nevertheless, these methods are computationally expensive, and generally underperform the first camp. A third group uses reinforcement learning (RL), formulating RNA design as a sequential decision-making problem (Eastman *et al.*, 2018; Runge *et al.*, 2019; Obonyo *et al.*, 2022). However, the performance of these vanilla RL systems trained from scratch lag behind strong heuristic designers.

In this work, we propose a fundamentally different perspective: RNA design as *conditional sequence generation*. Instead of solving a combinatorial optimization problem from scratch for each structure, we learn a

reusable (shared) *neural approximator solver*. We make the following contributions:

1. We formulate RNA design as conditional sequence generation using an autoregressive language model.
2. We devise a constrained decoding algorithm to ensure the validity of designs for the input structure.
3. We develop a unified framework combining pretraining, supervised learning (SL) on structure–sequence pairs, and reinforcement learning (RL) on selected structures to directly optimize folding success.
4. We show that, surprisingly, SL on random-induced structure–sequence pairs unrelated to the test data yield competitive results on the latter.
5. We develop methods to select a small subset of structures for efficient RL based on sample diversity.
6. We utilize fast parallel sampling of large amounts of designs on modern GPUs, and our best model (SL+RL) outperforms the state-of-the-art systems in key metrics on four test sets, while being $1.7\times$ faster.

2. Preliminaries: RNA Folding and Design

2.1. RNA Sequences and Structures

An RNA sequence \mathbf{x} of is a string of nucleotides $x_1 x_2 \dots x_n$, where $x_i \in \mathcal{N}$ and $\mathcal{N} \triangleq \{\text{A, C, G, U}\}$. A pseudoknot-free secondary structure \mathbf{y} is represented as a dot-bracket string of the same length. Each character $y_i \in \{\cdot, (,)\}$ indicates whether nucleotide x_i is unpaired, paired downstream, or paired upstream, respectively. Base pairs are restricted to Watson–Crick–Franklin or wobble pairs: $\mathcal{P} = \{\text{CG, GC, AU, UA, GU, UG}\}$. For a given sequence \mathbf{x} , its *ensemble* $\mathcal{Y}(\mathbf{x})$ consists of all possible secondary structures. In thermodynamic RNA folding models, *Gibbs free energy change* $\Delta G^\circ(\mathbf{x}, \mathbf{y})$ is used to characterize the stability of secondary structure $\mathbf{y} \in \mathcal{Y}(\mathbf{x})$. The lower the free energy $\Delta G^\circ(\mathbf{x}, \mathbf{y})$, the more stable the structure \mathbf{y} for \mathbf{x} . The structure with the *minimum free energy* is the most stable one in the ensemble, i.e., the *MFE structure*,

$$\text{MFE}(\mathbf{x}) \triangleq \underset{\mathbf{y} \in \mathcal{Y}(\mathbf{x})}{\text{argmin}} \Delta G^\circ(\mathbf{x}, \mathbf{y}). \quad (1)$$

Note that for most methods for secondary structure prediction, ties for argmin are broken arbitrarily when there are multiple lowest free energy structures. This issue was often neglected in the literature, but it deserves clarification here. To be precise, we define $\text{MFEs}(\mathbf{x}) \triangleq \{\mathbf{y} \mid \Delta G^\circ(\mathbf{x}, \mathbf{y}) = \min_{\mathbf{y}' \in \mathcal{Y}(\mathbf{x})} \Delta G^\circ(\mathbf{x}, \mathbf{y}')\}$ to be the *set of MFE structures* for \mathbf{x} . When $|\text{MFEs}(\mathbf{x})| = 1$, we say \mathbf{x} has a *unique MFE* (uMFE) structure.

The *partition function* $Q(\mathbf{x}) \triangleq \sum_{\mathbf{y} \in \mathcal{Y}(\mathbf{x})} e^{-\Delta G^\circ(\mathbf{x}, \mathbf{y})/RT}$ sums the contribution of all structures in the ensemble, where R is the molar gas constant and T is the absolute temperature. Accordingly, the Boltzmann probability of a sequence \mathbf{x} folding into a structure \mathbf{y} is defined as $p(\mathbf{y} \mid \mathbf{x}) = \frac{e^{-\Delta G^\circ(\mathbf{x}, \mathbf{y})/RT}}{Q(\mathbf{x})}$.

2.2. RNA Design Problem

Given a target structure \mathbf{y}^* , RNA design (inverse folding problem; Fig. 1) aims to find a suitable RNA sequence \mathbf{x} that can naturally and easily fold into \mathbf{y}^* , within the design space $\mathcal{X}(\mathbf{y}^*)$ of all valid sequences for \mathbf{y}^* :

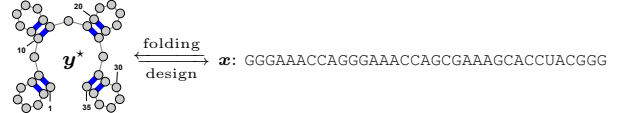


Fig. 1. RNA design is the inverse problem of RNA folding.

$$\mathcal{X}(\mathbf{y}^*) \triangleq \{\mathbf{x} \in \mathcal{N}^{|\mathbf{y}^*|} \mid \forall (i, j) \in \text{pairs}(\mathbf{y}^*), x_i x_j \in \mathcal{P}\} \quad (2)$$

We formulate the RNA design problem as optimizing a scoring function $f(\mathbf{x}, \mathbf{y}^*)$ over the design space $\mathcal{X}(\mathbf{y}^*)$:

$$\mathbf{x}^* = \underset{\mathbf{x} \in \mathcal{X}(\mathbf{y}^*)}{\text{argmax}} f(\mathbf{x}, \mathbf{y}^*) \quad (3)$$

where the scoring function quantifies how “easily” \mathbf{x} folds into \mathbf{y}^* . In practice, RNA design quality is evaluated using several standard metrics (Anderson-Lee et al., 2016; Zhou et al., 2023) which we adopt below. The first two (ensemble-based) are more important than the last two (MFE-based), because even if \mathbf{x} is an MFE solution there can still be many structures with similar energies, resulting in arbitrarily low probability of \mathbf{y}^* in ensemble.

- **Boltzmann probability** $p(\mathbf{y}^* \mid \mathbf{x})$ measures how likely \mathbf{x} folds into \mathbf{y}^* among all possible structures.
- **Normalized Ensemble Defect** $\text{NED}(\mathbf{x}, \mathbf{y}^*)$ quantifies how well the ensemble of structures formed by \mathbf{x} aligns with the target, penalizing competing folds (Zadeh et al., 2011a): $\text{NED}(\mathbf{x}, \mathbf{y}^*) = \frac{1}{|\mathbf{x}|} \sum_{\mathbf{y} \in \mathcal{Y}(\mathbf{x})} p(\mathbf{y} \mid \mathbf{x}) d_{\text{struct}}(\mathbf{y}^*, \mathbf{y})$, where $d_{\text{struct}}(\mathbf{y}, \mathbf{y}') \triangleq |\mathbf{y}| - 2 \cdot |\text{pairs}(\mathbf{y}) \cap \text{pairs}(\mathbf{y}')| - |\text{unpaired}(\mathbf{y}) \cap \text{unpaired}(\mathbf{y}')|$ is the structural distance.
- **MFE solution**: $f(\mathbf{x}, \mathbf{y}^*) = 1$ iff. $\mathbf{y}^* \in \text{MFEs}(\mathbf{x})$.
- **uMFE solution**: $f(\mathbf{x}, \mathbf{y}^*) = 1$ iff. $\text{MFEs}(\mathbf{x}) = \{\mathbf{y}^*\}$.

3. Models and Constrained Decoding

3.1. RNA Design as Conditional Seq. Generation

We frame RNA design as a conditional sequence generation task. Given a target secondary structure \mathbf{y}^* , we use an autoregressive language model $p_\theta(\cdot \mid \mathbf{y}^*)$ parameterized by θ that defines the conditional distribution

$$p_\theta(\mathbf{x} \mid \mathbf{y}^*) = \prod_{t=1}^n p_\theta(x_t \mid \mathbf{x}_{<t}, \mathbf{y}^*),$$

where $x_t \in \mathcal{N}$ is the nucleotide at position t and $\mathbf{x}_{<t}$ is the sequence prefix. This autoregressive factorization enables the model to condition each nucleotide decision on both the target structure and the previously generated prefix, capturing local dependencies that influence valid folding.

Vocabulary and input. We employ a compact, domain-specific vocabulary designed for structure-conditioned RNA generation. It consists of the four nucleotides (A, C, G, U), the three dot-bracket structure symbols ((,), .), and a small set of control tokens. The tokens `<struct>` and `</struct>` delimit the target structure, while `<bos>` and `<eos>` mark sequence boundaries. During inference, the structure is provided as a prefix prompt:

`<struct> (. (. . .)) </struct> <bos>`

after which the model autoregressively emits nucleotides until producing an `<eos>` token:

`G A C U U A G C <eos>`.

3.2. Constrained Decoding

Autoregressive generation with a language model does not, by default, respect the biochemical pairing rules required for a sequence to be compatible with a given RNA secondary structure. When decoding nucleotides token by token, the model may freely emit bases that violate Watson–Crick–Franklin or wobble pairing at positions that correspond to paired sites in \mathbf{y}^* , resulting in invalid sequences outside the valid design space $\mathcal{X}(\mathbf{y}^*)$. To mitigate this mismatch between vanilla language model generation and RNA thermodynamic constraints, we employ a *constrained decoding* mechanism that enforces base-pairing rules during generation.

In the aspect of formal language theory, our valid design space $\mathcal{X}(\mathbf{y}^*)$ is a **context-free language** (with long-distance dependencies) and needs a runtime stack to ensure valid decoding. However, our method below uses a (stack-based) precomputation to avoid the runtime stack, reducing the overhead.

Constraint rule. Let \mathbf{y}^* denote a dot–bracket structure. We precompute a mapping $m(t)$ that maps the index of each “)” to the index of its matching “(”. At decoding step t , the set of admissible nucleotides is defined as:

$$\mathcal{A}_t = \begin{cases} \{\text{A, C, G, U}\}, & y_t^* \in \{\cdot, \}\}, \\ \text{Comp}(x_{m(t)}), & y_t^* = \cdot \end{cases}$$

where $\text{Comp}(\cdot)$ lists the nucleotides compatible with pairing constraints, i.e., $\text{Comp}(\text{A}) = \{\text{U}\}$, $\text{Comp}(\text{C}) = \{\text{G}\}$, $\text{Comp}(\text{G}) = \{\text{C, U}\}$, and $\text{Comp}(\text{U}) = \{\text{A, G}\}$.

Implementation. At each decoding step, we mask the logits of all invalid nucleotides according to \mathcal{A}_t and renormalize: $\tilde{p}_\theta(x_t \mid \mathbf{x}_{<t}, \mathbf{y}^*) \propto \mathbf{1}_{[x_t \in \mathcal{A}_t]} p_\theta(x_t \mid \mathbf{x}_{<t}, \mathbf{y}^*)$. A lightweight callback computes \mathcal{A}_t on-the-fly from y_t^* and the nucleotide previously generated at its paired site. After position n has been filled, only `<eos>` remains valid, ensuring that the generated sequence length matches the target structure.

Effect. This decoding strategy guarantees structural validity by construction and reduces the effective search space from 4^n (regular language $\{\text{A, C, G, U}\}^n$) to $6^m 4^u$ (context-free language $\mathcal{X}(\mathbf{y}^*)$) for m base pairs and u unpaired positions. Its computational overhead is about 30% (see Fig. 6), yet it substantially improves sample efficiency and training stability in both supervised and reinforcement learning settings.

4. Language Model Training

4.1. Pretrained Model

Large language models trained on massive, diverse text corpora have been shown to acquire broad inductive biases that transfer surprisingly well beyond natural language (Touvron *et al.*, 2023; Yang *et al.*, 2024). Even relatively small decoder-only LMs develop stable attention patterns, long-range dependency modeling, and useful parameter initializations that make fine-tuning in downstream tasks significantly more data-efficient than training a transformer from scratch. Motivated by these observations, we begin with the Qwen2.5–0.5B (Yang

et al., 2024) pretrained model (GPT-style decoder-only Transformer) as the backbone for our RNA design system. Although the original training domain is textual, our experiments show that the pretrained backbone provides substantially better optimization stability and sample efficiency than a randomly initialized transformer of identical architecture. In ablations, the scratch-trained model converges more slowly and yields lower folding performance, confirming that the pretrained initialization is a critical component of our approach.

Surgery for RNA adaptation. To turn the general-domain LLM into an RNA-capable generator, we perform a minimal architectural modification. As illustrated in Fig. 2, we keep all transformer backbone layers intact and modify only the input and output layers. The original embedding matrix and LM head are removed, and we introduce downsized, RNA-specific replacements built around the vocabulary defined above. This preserves the pretrained backbone while enabling the model to process RNA tokens and structural prompts.

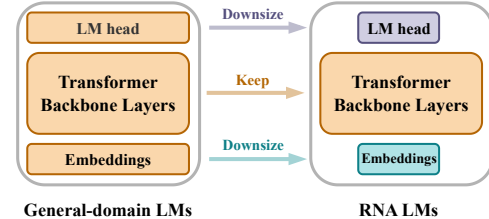


Fig. 2. We convert a general-domain LLM into an RNA designer by keeping the pretrained transformer backbone and shrinking the input and output layers. The original embedding and LM head are downsized and reinitialized to support RNA tokens.

Why not use existing RNA LMs? Several RNA-focused language models have been proposed, but they are not well suited to our setting (see also Sec. 7):

- Lack of structural input.** Existing RNA LMs typically operate only on nucleotide sequences and do not accept dot–bracket structures as input, preventing direct structure-conditioned generation for design.
- Architectural mismatch.** Most publicly available RNA LMs are BERT-style encoders rather than autoregressive decoders. A GPT-style RNA LM has been reported, but no usable checkpoint has been released (Xiao *et al.*, 2024).
- Tokenization mismatch.** Existing RNA LMs adopt subword or BPE-style tokenization (e.g., merging adjacent nucleotides into one token, as in some recent generative RNA LMs (Zhao *et al.*, 2024)). This breaks the one-nucleotide-per-token setting that our constrained decoding relies on, making it much harder to control the validity of the decoded sequence: base-pairing constraints can no longer be enforced easily.
- Software compatibility.** Many RNA LMs are implemented in standalone codebases or lack Hugging-Face compatibility, making integration with our constrained decoding and RL pipeline difficult.

Why not encoder-decoder models? Although RNA design can be formulated as encoder-decoder translation ($\mathbf{y}^* \rightarrow \mathbf{x}$), we adopt a decoder-only LM for high-throughput sampling and pretraining compatibility. Encoder-decoder models need to compute cross-attention at each decoding step (Vaswani *et al.*, 2017), which often dominates incremental decoding cost, limiting sampling throughput when generating many candidates per target (Lu *et al.*, 2024) (we use 10^4 samples). Moreover, conditioning via prefix prompting keeps supervised training and future RNA pretraining straightforward, and naturally supports mixing RNA sequences with sequence-structure pairs, whereas encoder-decoder pretraining on sequence-only data is not straightforward and requires denoising objectives or back-translation pipelines (Raffel *et al.*, 2020; Lewis *et al.*, 2020; Sennrich *et al.*, 2016).

4.2. Supervised Learning (SL)

To initialize the model, we construct a training corpus of structure-sequence pairs. Following the knowledge distillation paradigm, we employ a strong optimization-based solver, SAMFEO (Zhou *et al.*, 2023), to generate sequences for diverse target structures (see Sec. 5.2). The resulting dataset $\mathcal{YX}_{\text{train}}$ contains $\{(\mathbf{y}^*, \mathbf{x})\}$ pairs where each \mathbf{x} is a valid design for \mathbf{y}^* . The model is trained by maximum likelihood estimation (MLE):

$$\mathcal{L}_{\text{SL}}(\theta) = - \sum_{(\mathbf{y}^*, \mathbf{x}) \in \mathcal{YX}_{\text{train}}} \log p_{\theta}(\mathbf{x} \mid \mathbf{y}^*).$$

After SL, the model can rapidly generate many plausible designs, enabling efficient exploration in RL.

4.3. Reinforcement Learning (RL)

Supervised learning aligns the model with solver-generated sequences but does not directly optimize our thermodynamic objective (e.g., Boltzmann probability $p(\mathbf{y}^* \mid \mathbf{x})$ and ensemble defect $\text{ED}(\mathbf{x}, \mathbf{y}^*)$). We therefore fine-tune p_{θ} with a simple group-based REINFORCE-style objective (Williams, 1992), often referred to as *Group Relative Policy Optimization* (GRPO) (Shao *et al.*, 2024).

Given a target structure \mathbf{y}^* , we sample a group of K sequences $\{\mathbf{x}_k\}_{k=1}^K \sim p_{\theta}(\cdot \mid \mathbf{y}^*)$ (using constrained decoding) and compute rewards $R_k = R(\mathbf{x}_k, \mathbf{y}^*)$. We form a group baseline $b = \frac{1}{K} \sum_{k=1}^K R_k$ with standard deviation $\sigma = \text{Std}_k(R_k)$, and define a normalized advantage $\hat{A}_k = \frac{R_k - b}{\sigma + \epsilon}$. The GRPO loss is

$$\mathcal{L}_{\text{GRPO}}(\theta) = -\mathbb{E}_k [\hat{A}_k \log p_{\theta}(\mathbf{x}_k \mid \mathbf{y}^*)], \quad (4)$$

which increases the probability of better-than-average samples within each group and decreases that of worse-than-average ones, on top of the supervised initialization.

Reward Design. For reinforcement learning, we map the thermodynamic quantities in Section 2 to a single scalar reward that reflects how well a candidate sequence \mathbf{x} folds into the target structure \mathbf{y}^* . During RL, we always use constrained decoding (Section 3.2) so that sampled sequences satisfy the length and base-pairing constraints of $\mathcal{X}(\mathbf{y}^*)$; the reward is therefore defined over $\mathbf{x} \in \mathcal{X}(\mathbf{y}^*)$.

Reward components. For each sampled pair $(\mathbf{x}, \mathbf{y}^*)$, we call an RNA folding engine to obtain the Boltzmann

probability $p(\mathbf{y}^* \mid \mathbf{x})$, the set of MFE structures $\text{MFEs}(\mathbf{x})$, and whether the MFE is unique. Let $\mathbb{I}[\cdot]$ denote the indicator function. We define three reward components:

$$\begin{aligned} r_{\text{prob}}(\mathbf{x}, \mathbf{y}^*) &= p(\mathbf{y}^* \mid \mathbf{x}), \quad r_{\text{mfe}}(\mathbf{x}, \mathbf{y}^*) = \mathbb{I}[\mathbf{y}^* \in \text{MFEs}(\mathbf{x})], \\ r_{\text{umfe}}(\mathbf{x}, \mathbf{y}^*) &= \mathbb{I}[\mathbf{y}^* \in \text{uMFE}(\mathbf{x})]. \end{aligned} \quad (5)$$

The first term rewards sequences whose Boltzmann ensemble is concentrated on the target structure. The second term adds a bonus whenever the target structure appears among the MFE structures of \mathbf{x} . The third term further rewards sequences whose MFE structure is unique, discouraging strong competing alternative folds. Here $\text{uMFE}(\mathbf{x})$ denotes the unique MFE structure if it exists and the empty set otherwise.

Combined reward. We combine the three rewards with simple linear shaping:

$$\begin{aligned} R(\mathbf{x}, \mathbf{y}^*) &= 0.5 r_{\text{prob}}(\mathbf{x}, \mathbf{y}^*) + 0.25 r_{\text{mfe}}(\mathbf{x}, \mathbf{y}^*) \\ &\quad + 0.25 r_{\text{umfe}}(\mathbf{x}, \mathbf{y}^*), \quad \mathbf{x} \in \mathcal{X}(\mathbf{y}^*). \end{aligned} \quad (6)$$

By construction, $r_{\text{prob}} \in [0, 1]$ and $r_{\text{mfe}}, r_{\text{umfe}} \in [0, 0.5]$, so $R(\mathbf{x}, \mathbf{y}^*) \in [0, 1]$ and $R(\mathbf{x}, \mathbf{y}^*) = 1$ exactly when the target structure has probability 1 and is the unique MFE structure. If the thermodynamic evaluation fails for numerical or library-related reasons, we fall back to a neutral reward $R(\mathbf{x}, \mathbf{y}^*) = 0$, so such rare cases neither strongly encourage nor discourage the policy.

5. Datasets Construction

5.1. Test Dataset $\mathcal{Y}_{\text{test}}$

For RNA design, the test set $\mathcal{Y}_{\text{test}}$ is a collection of target structures \mathbf{y}^* . We create a comprehensive test set consisting of four datasets, covering both manually-designed puzzles and native structures:

1. **Eterna100** (Anderson-Lee *et al.*, 2016) is the standard and most widely used benchmark for evaluating RNA design programs. It contains 100 secondary structures (i.e., human-designed “puzzles”) of up to 400 nt, varying in design difficulty from simple hairpins to intricate multiloop structures.
2. **Eterna100-v2** (Koodli *et al.*, 2021) modifies 19 puzzles from Eterna100 so that all puzzles are MFE-solvable under Turner 2004 energy model (Mittal *et al.*, 2024) via ViennaRNA v2 (Lorenz *et al.*, 2011).
3. **Rfam-Taneda-27** (Taneda, 2011) includes consensus secondary structures from seed alignments in Rfam 9.0, with each entry corresponding to an RNA family.
4. **RNA solo-100**, extracted from (Adamczyk *et al.*, 2022), is a collection of secondary structures curated from a database of experimentally determined RNA 3D structures. The specific “100” subset here refers to 100 cleaned, non-redundant RNA structures we selected for secondary-structure-design benchmarking.

We call the set of unique structures from all four datasets our “**Union Test Set**”, notated $\mathcal{Y}_{\text{test}}$, which contains 246 unique structures, with length up to 400 nt.

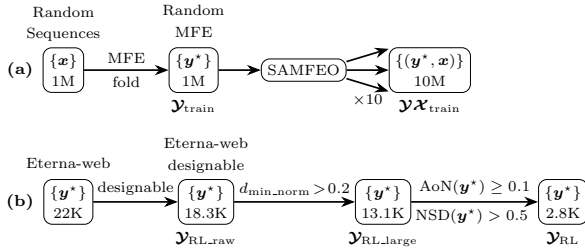


Fig. 3. Workflows for constructing (a) SL and (b) RL training datasets. Here, $d_{\min, \text{norm}}$ denotes $d_{\min, \text{norm}}(\mathbf{y}^*, \mathbf{y}'_{\text{test}})$.

5.2. Supervised Learning Dataset $\mathbf{yX}_{\text{train}}$

Our supervised training dataset $\mathbf{yX}_{\text{train}}$ is a set of $(\mathbf{y}^*, \mathbf{x})$ pairs where each \mathbf{y}^* is a target structure (i.e., a puzzle) and each \mathbf{x} is the corresponding RNA sequence (i.e., a design). We construct this set in two steps: (a) collect the set of target structures $\mathbf{y}_{\text{train}}$, and then (b) use a state-of-the-art tool to generate candidate designs for each structure in $\mathbf{y}_{\text{train}}$.

For step (a), while previous work used native or native-derived structures such as Rfam-Learn (Runge *et al.*, 2019), those data suffers from three serious drawbacks:

1. **Testset contamination:** the test set contains native structures that are too similar to some native or native-derived ones in the training set;
2. **Limited size:** native structures are often limited in quantity (e.g., Rfam-Learn has only 65K structures), which may not provide enough training data for the data-hungry Transformer language models.
3. **Limited diversity:** many native sequences are homologous ones from the same families (e.g., Rfam-Learn is derived from Rfam, a collection of native RNA sequences by families), where sequences and structures in each family share high sequence identities and structural similarities.

To addresses these issues, we instead propose to use large amounts of randomly generated (and thus diverse) artificial structures unrelated to the test sets. However, directly generating random secondary structures is problematic, as most of them will be undesignable in the MFE criteria (Zhou *et al.*, 2024). Instead, we first generated 1M random RNA sequences of lengths up to 500 nt, with uniform distribution of nucleotides {A, C, G, U}, and then use ViennaRNA v2 to get their MFE structures; now we have 1M random-MFE structures in $\mathbf{y}_{\text{train}}$ (see Fig. 3(a)). This way we made sure all these structures are designable by the MFE criterion.¹

For each target structure in $\mathbf{y}_{\text{train}}$, we use the state-of-the-art SAMFEO tool to generate 10 candidate designs, so finally we have 10M $(\mathbf{y}^*, \mathbf{x})$ pairs in $\mathbf{yX}_{\text{train}}$. Surprisingly, this random-induced supervised dataset unrelated to the test set yields competitive results on the latter (Sec. 6.1).

5.3. Reinforcement Learning Dataset \mathbf{y}_{RL}

It is a general consensus in language model training that the later the training stage, the less data is needed (with more compute per example), but with higher quality

standards. Given that RL is the last stage in training, we construct a small and relevant dataset \mathbf{y}_{RL} in three steps. It is important to note that, different from supervised learning, RL only needs structures \mathbf{y}^* , but not solutions \mathbf{x} , since it will explore possible solutions via decoding.

Step 1. data source: Eterna-web. We first downloaded the full collection of 22K player-designed structures (i.e., puzzles) from the Eterna website (<http://eternagame.org>), excluding those from Eterna100. We then removed structures longer than 500 nt (to match test sets), and removed MFE-undesignable ones using our previous work (Zhou *et al.*, 2024), which resulted in 18.3K MFE-designable structures ($\mathbf{y}_{\text{RL, raw}}$ in Fig. 3(b)).

Step 2. Removing structures similar to test data. Unlike our SL training set $\mathbf{yX}_{\text{train}}$ of random-induced structures that are unrelated to our test data, our RL set is drawn from a distribution similar to one of our testsets (Eterna100), so potentially there is a risk of testset contamination. To ensure a rigorous evaluation, we removed structures $\mathbf{y}^* \in \mathbf{y}_{\text{RL, raw}}$ that were too close to any test structure \mathbf{y}' in \mathbf{y}_{test} . For each \mathbf{y}^* , we computed a *normalized minimum edit distance* that accounts for length differences:

$$d_{\min, \text{norm}}(\mathbf{y}^*, \mathbf{y}_{\text{test}}) = \min_{\mathbf{y}' \in \mathbf{y}_{\text{test}}} \frac{d_{\text{edit}}(\mathbf{y}^*, \mathbf{y}')}{\min(|\mathbf{y}^*|, |\mathbf{y}'|)}.$$

Here, $d_{\text{edit}}(\cdot, \cdot)$ denotes the edit distance between two structures, and normalization by the length of the shorter structure $\min(|\mathbf{y}^*|, |\mathbf{y}'|)$ ensures that our similarity measure is comparable across structures of different lengths. Structures in $\mathbf{y}_{\text{RL, raw}}$ with a $d_{\min, \text{norm}}(\mathbf{y}^*, \mathbf{y}_{\text{test}})$ 0.2 or less (i.e., 80%+ similar) were excluded to prevent information leakage between RL and test sets (Fig. 4(a)), resulting in 13.1K structures ($\mathbf{y}_{\text{RL, large}}$ in Fig. 3(b)).

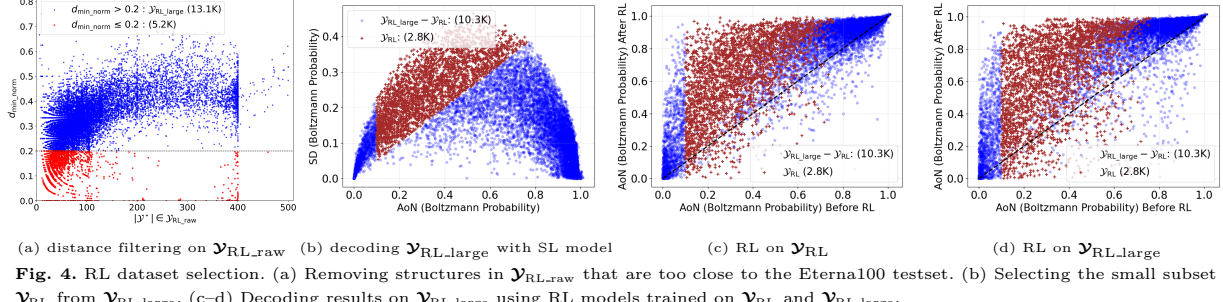
Step 3. Further filtering for RL efficiency and quality. We could do RL on the above $\mathbf{y}_{\text{RL, large}}$ set, but it is computationally expensive because, for each target structure the model must generate many samples (“exploration”) and evaluate their folding performance. Our goal is to identify a small subset $\mathbf{y}_{\text{RL}} \subseteq \mathbf{y}_{\text{RL, large}}$ for which RL is likely to yield meaningful improvement.

To do so, we first decode structures in $\mathbf{y}_{\text{RL, large}}$ with the SL model trained on $\mathbf{yX}_{\text{train}}$. For each structure \mathbf{y}^* in $\mathbf{y}_{\text{RL, large}}$, we generate K candidate sequences $\{\mathbf{x}_k\}_{k=1}^K$ and compute their Boltzmann probabilities $p(\mathbf{y}^* | \mathbf{x}_k)$. We then summarize the distribution of these probabilities with two statistics:

- **Average probability (AoN):** $\text{AoN}(\mathbf{y}^*) = \frac{1}{K} \sum_{k=1}^K p(\mathbf{y}^* | \mathbf{x}_k)$, which reflects the performance of the SL model for structure in terms of the ensemble metric $p(\mathbf{y}^* | \mathbf{x}_k)$.
- **Standard deviation of probabilities:** $\text{SD}(\mathbf{y}^*) = \text{Std}_k(p(\mathbf{y}^* | \mathbf{x}_k))$ capturing the variability, and hence the potential for improvement across sampled designs.

Using $\text{SD}(\mathbf{y}^*)$ alone can be misleading for structures whose probabilities remain uniformly low. Thus, we propose the *normalized standard deviation* (NSD): $\text{NSD}(\mathbf{y}^*) = \frac{\text{SD}(\mathbf{y}^*)}{\text{AoN}(\mathbf{y}^*)}$, which expresses variability relative to the mean probability and highlights structures where RL can exploit useful diversity in folding outcomes.

¹ Although some of $\mathbf{y}_{\text{train}}$ might not be uMFE-designable.



Selection criteria. We select a structure \mathbf{y}^* from \mathcal{Y}_{train} for reinforcement learning if

$$AoN(\mathbf{y}^*) \geq 0.1 \text{ and } NSD(\mathbf{y}^*) > 0.5. \quad (7)$$

The AoN threshold removes structures on which the SL model performs extremely poorly, while the NSD threshold ensures that there is sufficient variance among sampled sequences for RL to meaningfully refine the model. Applying both criteria yields a filtered subset \mathcal{Y}_{RL} of approximately 2.8K structures (Fig. 4(b)) on which RL is both computationally feasible and empirically effective. Moreover, Fig. 4(c-d) compare AoN scores before and after RL when training on either the full set \mathcal{Y}_{RL_large} or the filtered subset \mathcal{Y}_{RL} . When RL is applied to the entire \mathcal{Y}_{RL_large} , many structures in \mathcal{Y}_{RL_large} actually exhibit degraded performance after RL. In contrast, when RL is restricted to \mathcal{Y}_{RL} , the model not only improves performance on most structures in \mathcal{Y}_{RL} but also generalizes positively, yielding improvements for many structures in \mathcal{Y}_{RL_large} as well. These results confirm that our filtering yields a small subset that improves both the efficiency and quality of RL training. Sec. 6.4 further showed a $\sim 2.9\times$ speedup by RL on \mathcal{Y}_{RL} (16 hours vs. 47 hours of RL on \mathcal{Y}_{RL_large}).

6. Evaluation Results

6.1. Supervised Learning Results

Figure 5(a) reports the best-of- N Boltzmann probability achieved by each supervised-learning (SL) model trained on our 10M \mathcal{YX}_{train} set as a function of the number of decoded samples N per target structure. Across all sampling budgets, the pretrained Qwen-0.5B-SL model performs the strongest after SL, reaching a best-of- N probability of approximately 0.55 at $N = 10^4$. By contrast, both models trained from scratch, Qwen-0.5B-SL_Scratch (decoder-only) and T5-0.7B-SL_Scratch (encoder-decoder), perform substantially worse. These results clearly suggest that training Transformer LMs for RNA design entirely from scratch is ineffective regardless of architecture. The Target_Initialization is a simple baseline where for each unpaired position in \mathbf{y}^* , we use a distribution of 90% A (other nucleotides for the remaining 10%) and for each basepair in \mathbf{y}^* , we use a distribution of 70% GC/CG pairs, 40% AU/UA pairs, and 10% Wobble pairs. This baseline performs surprisingly well and even surpasses both T5 models at moderate sampling

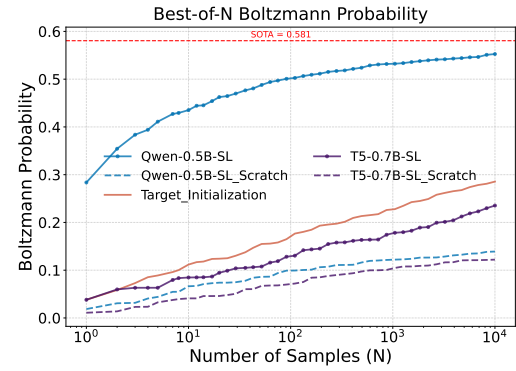


Fig. 5. Supervised learning results of different models trained on \mathcal{YX}_{train} in terms of best-of- N Boltzmann probability on Eternal100.

budgets. Although it ultimately is far below the best model, its competitiveness underscores the limitations of uninitialized models in capturing structural constraints.

On the other hand, it is surprising and encouraging that supervised training on random-induced structure-sequence pairs \mathcal{YX}_{train} which are completely unrelated to the test set can perform reasonably well on the latter.

6.2. Decoding: Constrained vs. Unconstrained

We empirically compare naive decoding and constrained decoding on the union test set \mathcal{Y}_{test} using the SL-trained Qwen2.5-0.5B-SL model. For each target structure, we draw 10^3 samples with both decoding methods and for every decoded sequence, record (i) structural invalidity (any base pair in \mathbf{y}^* violating Watson-Crick-Franklin or wobble rules), and (ii) wall-clock decoding time.

As shown in Fig. 6, naive decoding yields a sharp rise in invalid sequences as target length increases, wasting a substantial fraction of samples. In contrast, constrained decoding eliminates invalid outputs by design, while incurring a modest $\sim 30\%$ overhead. This modest overhead is more than offset by the improved effective sample efficiency, so we adopt constrained decoding in RL.

Fig. S5 additionally shows an attention map from constrained decoding, which correlates with base-pairs \mathbf{y}^* .

6.3. Reinforcement Learning Results

Fig. 7 shows that applying reinforcement learning (RL) on top of the supervised-learning (SL) model leads to a substantial improvement in best-of- N Boltzmann probability across all three benchmarks. The RL-enhanced model consistently outperforms the SL-only model, with

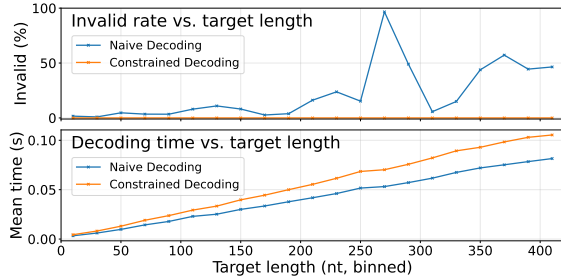


Fig. 6. Naive decoding vs. constrained decoding on the Union Test Set $\mathcal{Y}_{\text{test}}$ (10^3 samples per structure; supervised learning model). Naive decoding becomes increasingly invalid for longer targets, while constrained decoding guarantees validity at a $\sim 30\%$ slowdown.

Method	Eterna100				RNAsolo100			
	$p(\mathbf{y}^* \mathbf{x})$	NED _↓	MFE	uMFE	$p(\mathbf{y}^* \mathbf{x})$	NED _↓	MFE	uMFE
RNAinverse-pf	0.571	0.045	77	72	0.710	0.015	79	79
NEMO	0.271	0.098	79	77	0.506	0.038	81	81
SAMFEO	0.580	0.043	77	74	0.723	0.013	80	79
Ours: SL+RL	0.586	0.042	74	72	0.728	0.013	81	81

Method	Eterna100-v2				Rfam-Taneda-27			
	$p(\mathbf{y}^* \mathbf{x})$	NED _↓	MFE	uMFE	$p(\mathbf{y}^* \mathbf{x})$	NED _↓	MFE	uMFE
RNAinverse-pf	0.590	0.039	82	77	0.808	0.004	24	24
NEMO	0.270	0.098	90	87	0.411	0.025	25	25
SAMFEO	0.596	0.036	83	79	0.809	0.004	24	24
Ours: SL+RL	0.606	0.036	81	79	0.818	0.039	24	24

Table 1. Comparison with state-of-the-art systems on all four test sets. RNAinverse-pf was updated in ViennaRNA 2.6 (2023). Our results report the best of 10^4 samples.

particularly large gains on Eterna100 and Rfam-Taneda-27, where the performance gap remains pronounced for all sampling budgets. RL greatly improves sample efficiency especially on Rfam-Taneda-27, where only 15 samples are needed to surpass SAMFEO in Boltzmann probability.

Overall, these results demonstrate that RL significantly strengthens the model’s ability to generate high-probability designs, especially for benchmarks involving complex or human-designed structures, and consistently improves the scaling behavior of the SL baseline. Similarly, from Table 1, we observe that our reinforcement-fine-tuned model consistently matches or surpasses other methods on ensemble-based metrics. It also achieves the best performance on $p(\mathbf{y}^* | \mathbf{x})$ across all datasets and attains the best NED—tied only with SAMFEO on RNAsolo100, while outperforming RNAinverse-pf (updated in 2023) and NEMO on all datasets for both $p(\mathbf{y}^* | \mathbf{x})$ and NED. Similarly, our SL+RL model also demonstrates high sample efficiency in generating MFE solutions. As shown in Fig. S1, our model requires only 2 samples on Rfam-Taneda-27 and 50 samples on RNAsolo100 to match the performance of the state-of-the-art method.

Fig. S4 presents an comparison of Boltzmann probabilities between SAMFEO (Sota) and Ours (SL+RL) model on the Eterna100 test set. Each point corresponds to a puzzle, and the size of the “+” marker reflects the structure length, with larger markers indicating longer puzzles. Our approach consistently achieves higher probabilities, particularly for longer and hard-to-design puzzles. The zoomed-in region highlights the most

challenging puzzles, where our model shows the most substantial advantage over SAMFEO.

6.4. Efficiency

On a single NVIDIA H100 GPU, our model based on Qwen2.5-0.5B requires 50 hours of supervised learning (SL) on the 10M structure-sequence pairs $(\mathbf{y}, \mathbf{x})_{\text{train}}$, and 16 and 47 hours of reinforcement learning (RL) on \mathcal{Y}_{RL} and $\mathcal{Y}_{\text{RL,large}}$ (2.8K and 13.1K structures), respectively.

While training might be slow, decoding is fast even with large sample size (10^4). Fig. 8 reports decoding time on Eterna100 as a function of structure length. Our method (98% compute on GPUs and 2% on CPU to evaluate the decoded sequence) is consistently faster than the SOTA tool SAMFEO (with 5 parallelized runs on CPUs), and has a slower empirical complexity (roughly $|y|^{1.3}$ vs. $|y|^{1.9}$). Overall, our approach yields a $1.74\times$ speedup.

7. Related Work

RNA LMs for RNA Analysis. Several recent studies train BERT-style encoders on large RNA corpora for downstream structure-prediction and analysis, including RNABERT, RNA-FM, RNA-MSM, and RiNALMo (Akiyama and Sakakibara, 2022; Chen et al., 2022; Zhang et al., 2023; Penić et al., 2025). Benchmarks (Zablocki et al., 2025) show that such RNA LMs improve analysis, but they (a) operate on RNA sequences without structure tokens, and (b) are encoder-only architectures and thus incapable of *de novo* design. By contrast, we use a decoder-only LM that conditions on dot-bracket structures and is trained end-to-end to *generate* RNA sequences, with constrained decoding and RL explicitly targeting folding success.

Generative Models for RNA Generation. Deep generative models have recently been explored for RNA sequence design. GAN- and VAE-style approaches such as RNAGEN and RfamGen generate family- or target-specific RNAs (Ozden et al., 2023; Sumi et al., 2024). Closer to our setting, GenerRNA is an autoregressive LM pretrained on large-scale RNA data and fine-tuned to generate functional (e.g., protein-binding) RNAs but without conditioning on an explicit input (Zhao et al., 2024). RNATranslator models protein-conditional RNA design as a sequence-to-sequence problem, where an encoder processes a protein sequence and a decoder generates RNA binders (Shukueian Tabrizi et al., 2025). Our LM differs from these generative approaches in three ways. First, we condition directly on secondary structures. Second, we enforce base-pairing constraints via constrained decoding rather than filtering post hoc. Third, we fine-tune the LM with RL on rewards that align with standard RNA design objectives.

Reinforcement Learning for RNA Design. RL provides an appealing framework for RNA design by framing it as a sequential decision process: at each step, an agent chooses an action (an edit on the sequence) and receives a reward based on how well the new sequence folds to the target structure. Eastman et al. (2018) pioneered this idea, with each state being a full sequence and each action being an edit on one or two nucleotides. Runge et al. (2019) introduced LEARNA and Meta-LEARNA,

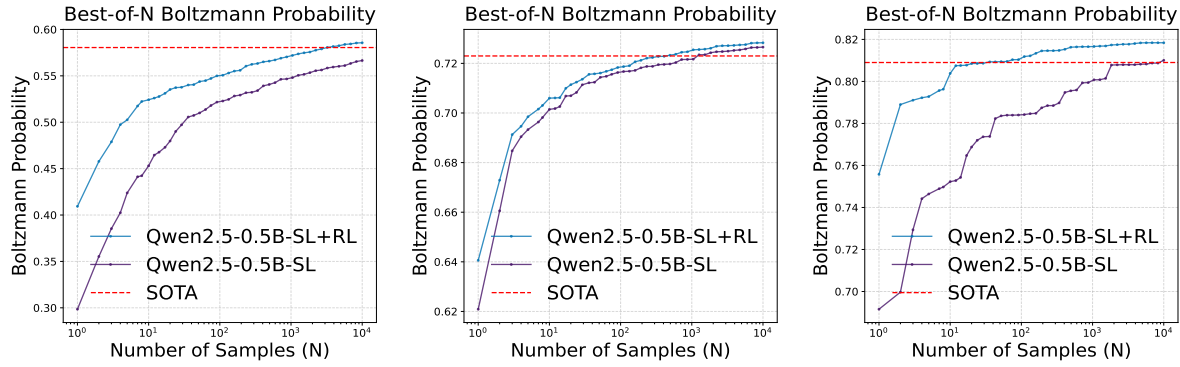


Fig. 7. Best-of- N probability curves for the SL and SL+RL models on three test sets. In all cases, RL brought substantial improvements over SL, surpassing SOTA (SAMFEO); in particular, RL only needs ~ 15 samples to surpass SAMFEO in (c). See Fig. S3 for other metrics.

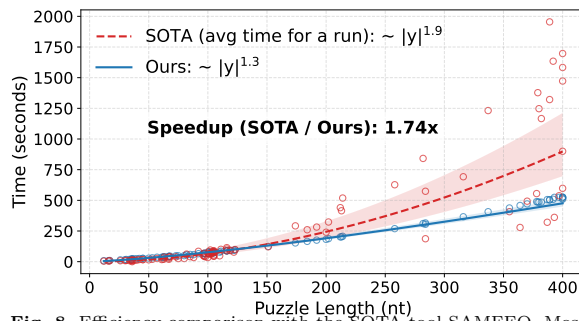


Fig. 8. Efficiency comparison with the SOTA tool SAMFEO. Most of our runtime is on GPUs (only 2% is on CPU). Ours is 1.7 \times faster.

where each state is a partial sequence and each action is to add one unpaired or two paired nucleotides. Obonyo *et al.* (2022) proposed RNAsp, a self-play RL framework inspired by AlphaZero. Partial RNA design (Runge *et al.*, 2024) extends LEARNA to handle sequence constraints.

Our use of RL is complementary and operates in a different regime. Rather than training a task-specific RL agent from scratch, we fine-tune a *single* structure-conditioned LM that has already been trained by supervised learning on solver-generated examples. As a result, our model acts as an amortized neural solver: once trained, it can rapidly generate high-quality designs for new targets without per-instance RL optimization, while still benefiting from RL's ability to directly optimize folding-based rewards (see also Tab. S1).

8. Conclusions and Future Work

We have presented the first study of using autoregressive language models for RNA design (inverse folding). Combining pretraining, constrained decoding, supervised learning, and reinforcement learning, our final model outperforms (or ties with) the state-of-the-art in ensemble-based metrics across all four datasets, while being 1.7 \times faster. We also constructed and released carefully curated datasets for SL and RL training and testing, which will benefit future studies.

Our work can be improved in the following ways:

- Our decoding algorithm is sampling with context-free constraints. Since we need to sample a large amount of designs both for reinforcement learning and for testing, decoding speed need improvement. First, we can use other decoding algorithms such as beam search (Huang

et al., 2017). Secondly, the $\sim 30\%$ overhead due to constraints could be reduced by advanced techniques for LM generation of context-free languages (Dong *et al.*, 2024).

- Currently, reinforcement learning is still slow, limiting us to a small sample size. Once decoding speed improves, we can afford to do better reinforcement learning with more data and more exploration.
- Finally, we can explore Test-Time Reinforcement Learning (TTRL) methods (Zuo *et al.*, 2025) to train a different model for each testing structure, further exploiting test-time scaling.

References

Adamczyk, B., Antczak, M. and Szachniuk, M. (2022). Rnasolo: a repository of cleaned PDB-derived RNA 3d structures. *Bioinformatics*, **38**(15), 3668–3670.

Akiyama, M. and Sakakibara, Y. (2022). Informative RNA base embedding for RNA structural alignment and clustering by deep representation learning. *NAR Genom. Bioinf.*, **4**(1).

Anderson-Lee, J., Fisker, E., Kosaraju, V., Wu, M., Kong, J., Lee, J., Lee, M., Zada, M., Treuille, A. and Das, R. (2016). Principles for predicting RNA secondary structure design difficulty. *J. Mol. Biol.*, **428**(5).

Andronescu, M., Fejes, A. P., Hutter, F., Hoos, H. H. and Condon, A. (2004). A New Algorithm for RNA Secondary Structure Design. *J. Mol. Biol.*, **336**(3).

Bachellerie, J. P., Cavallé, J. and Hüttenhofer, A. (2002). The expanding snoRNA world. *Biochimie*, **84**(8).

Bauer, G. and Suess, B. (2006). Engineered riboswitches as novel tools in molecular biology. *J. Biotech.*, **124**(1).

Bonnet, É., Rzazewski, P. and Sikora, F. (2020). Designing RNA secondary structures is hard. *J. Comp. Bio.*, **27**.

Chen, J., Hu, Z. and others (2022). Interpretable RNA Foundation Model from Unannotated Data for Highly Accurate RNA Structure and Function Predictions. *bioRxiv*.

Dong, Y., Ruan, C. and others (2024). Xgrammar: Flexible and efficient structured generation engine for large language models. *arXiv:2411.15100*.

Dotu, I., Garcia-Martin, J. A., Slinger, B. L., Mechery, V., Meyer, M. M. and Clote, P. (2014). Complete RNA inverse folding: computational design of functional

hammerhead ribozymes. *Nucleic Acids Res.*, **42**(18).

Doudna, J. A. Cech, T. R. (2002). The chemical repertoire of natural ribozymes. *Nature*, **418**(6894), 222–228.

Eastman, P. K., Shi, J., Ramsundar, B. and Pande, V. S. (2018). Solving the RNA design problem with reinforcement learning. *PLoS Comput. Biol.*, **14**(6).

Eddy, S. R. (2001). Non-coding RNA genes and the modern RNA world. *Nat. Rev. Genetics*, **2**(12).

Findeiß, S., Etzelt, M., Will, S., Mörl, M. and Stadler, P. F. (2017). Design of artificial riboswitches as biosensors. *Sensors*, **17**(9), 1990.

Garcia-Martin, J., Clote, P. and Dotu, I. (2013). RNAiFOLD: a constraint programming algorithm for RNA inverse folding and molecular design. *J. Bioinform. Comput. Biol.*, **11**(02).

Hamada, M. (2018). In silico approaches to RNA aptamer design. *Biochimie*, **145**, 8–14.

Hofacker, I., Fontana, W. and others (1994). Fast folding and comparison of RNA secondary structures. *Monatshefte für chemie*, **125**.

Huang, L., Zhao, K. and Ma, M. (2017). When to finish? optimal beam search for neural text generation (modulo beam size). In *Proc. EMNLP*.

Koodli, R., Schürch, F., Kladwang, W. and Das, R. (2021). Redesigning the EteRNA100 for the Vienna 2 Folding Engine. *bioRxiv*.

Lewis, M., Liu, Y., Goyal, N., Ghazvininejad, M., Mohamed, A., Levy, O., Stoyanov, V. and Zettlemoyer, L. (2020). BART: denoising sequence-to-sequence pre-training for natural language generation, translation, and comprehension. In *Proc. ACL*.

Lorenz, R., Bernhart, S. and others (2011). ViennaRNA Package 2.0. *Alg. Mol. Bio.*, **6**(1).

Lu, B.-R., Haduong, N., Lin, C.-Y., Cheng, H., Smith, N. A. and Ostendorf, M. (2024). Efficient encoder-decoder transformer decoding for decomposable tasks. *arXiv preprint arXiv:2403.13112*.

Mittal, A., Turner, D. H. and Mathews, D. H. (2024). NNDB: an expanded database of nearest neighbor parameters for predicting stability of nucleic acid secondary structures. *J. Mol. Biol.*, **436**(17).

Obonyo, S., Jouandeau, N. and Owuor, D. (2022). Designing RNA sequences by self-play. In *Proc. NCTA*.

Ozden, F., Barazandeh, S. and others (2023). RNAGEN: A generative adversarial network-based model to generate synthetic RNA sequences to target proteins. *bioRxiv*.

Penić, R. J., Vlašić, T., Huber, R. G., Wan, Y. and Šikić, M. (2025). RiNALMo: general-purpose RNA language models can generalize well on structure prediction tasks. *Nat. Commun.*, **16**(1), 5671.

Portela, F. (2018). An unexpectedly effective Monte Carlo technique for the RNA inverse folding problem. *bioRxiv*.

Raffel, C., Shazeer, N. and others (2020). Exploring the limits of transfer learning with a unified text-to-text transformer. *JMLR*, **21**.

Runge, F., Stoll, D., Falkner, S. and Hutter, F. (2019). Learning to design RNA. In *Proc. ICLR*.

Runge, F., Franke, J., Fertmann, D., Backofen, R. and Hutter, F. (2024). Partial RNA design. *Bioinfo.*, **40**.

Schwab, R., Ossowski, S., Riester, M., Warthmann, N. and Weigel, D. (2006). Highly specific gene silencing by artificial microRNAs in Arabidopsis. *Plant Cell*, **18**.

Sennrich, R., Haddow, B. and Birch, A. (2016). Improving neural machine translation models with monolingual data. In *Proc. ACL*.

Shao, Z., Wang, P. and others (2024). DeepSeekMath: Pushing the Limits of Mathematical Reasoning in Open Language Models. *arXiv 2402.03300*.

Shukueian Tabrizi, S., Barazandeh, S., Hashemi Aghdam, H. and Cicek, A. E. (2025). RNATranslator: Modeling protein-conditional RNA design as sequence-to-sequence natural language translation. *PLOS Comp. Bio.*, **21**.

Sumi, S., Hamada, M. and Saito, H. (2024). Deep generative design of RNA family sequences. *Nat. Methods*, **21**(3), 435–443.

Taneda, A. (2011). MODENA: a multi-objective RNA inverse folding. *Adv. Appl. Bioinform. Chem.*, **4**, 1.

Touvron, H., Lavril, T. and others (2023). Llama: Open and efficient foundation language models. *arXiv 2302.13971*.

Vaswani, A., Shazeer, N., Parmar, N., Uszkoreit, J., Jones, L., Gomez, A. N., Kaiser, L. and Polosukhin, I. (2017). Attention is all you need. In *Proc. NIPS*.

Williams, R. J. (1992). Simple statistical gradient-following algorithms for connectionist reinforcement learning. *Mach. Learn.*, **8**, 229–256.

Xiao, Y., Sun, E., Jin, Y. and Wang, W. (2024). RNA-GPT: multimodal generative system for RNA sequence understanding. *arXiv 2411.08900*.

Yamagami, R., Kayedkhordeh, M., Mathews, D. H. and Bevilacqua, P. C. (2018). Design of highly active double-pseudoknotted ribozymes: a combined computational and experimental study. *Nucleic Acids Res.*, **47**(1).

Yang, A., Yang, B. and others (2024). Qwen2.5 technical report. *arXiv:2412.15115*.

Zablocki, L., Bugnon, L. and others (2025). Comprehensive benchmarking of large language models for RNA secondary structure prediction. *Brief. Bioinfo.*, **26**(2).

Zadeh, J. N., Wolfe, B. R. and Pierce, N. A. (2011a). Nucleic acid sequence design via efficient ensemble defect optimization. *J. Comp. Chem.*, **32**(3).

Zadeh, J. N., Steenberg, C. D., Bois, J. S., Wolfe, B. R., Pierce, M. B., Khan, A. R., Dirks, R. M. and Pierce, N. A. (2011b). NUPACK: Analysis and design of nucleic acid systems. *J. Comp. Chem.*, **32**(1).

Zhang, Y., Lang, M. and others (2023). Multiple sequence alignment-based RNA language model and its application to structural inference. *Nucleic Acids Res.*, **52**(1).

Zhao, Y., Oono, K., Takizawa, H. and Kotera, M. (2024). GenerRNA: A generative pre-trained language model for de novo RNA design. *PLOS ONE*, **19**(10), 1–18.

Zhou, T., Dai, N., Li, S., Ward, M., Mathews, D. H. and Huang, L. (2023). RNA design via structure-aware multifrontier ensemble optimization. *Bioinfo.*, **39**.

Zhou, T., Tang, W. Y., Mathews, D. H. and Huang, L. (2024). Undesignable RNA Structure Identification via Rival Structure Generation and Structure Decomposition. *Proceedings of RECOMB*.

Zuo, Y. others (2025). TTTR: Test-time reinforcement learning. *arXiv:2504.16084*.

Appendix: Designing RNAs with Language Models

M. Gautam, N. Dai, T. Zhou, B. Xie, D. Mathews, and L. Huang
Oregon State University and University of Rochester

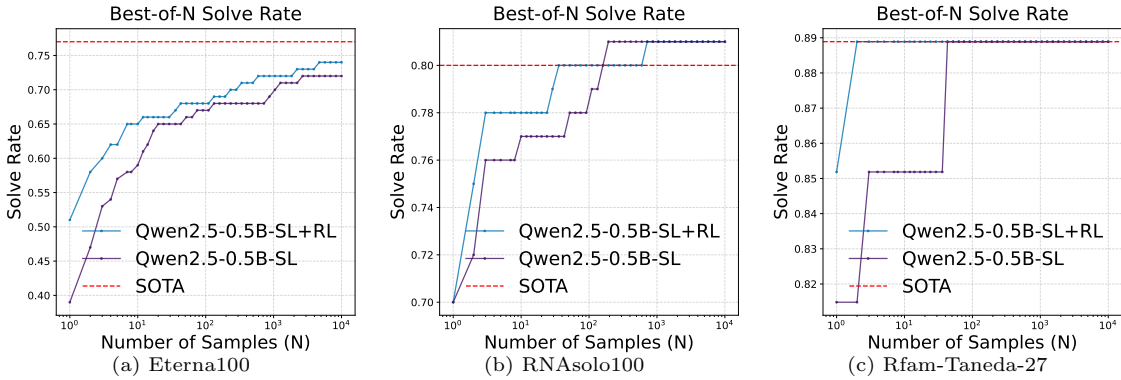


Fig. S1. Best-of- N curves for SL and SL+RL models in terms of MFE solve rate on three data sets. See Fig. 7 in the main text for the corresponding Best-of- N curves on Boltzmann probability.

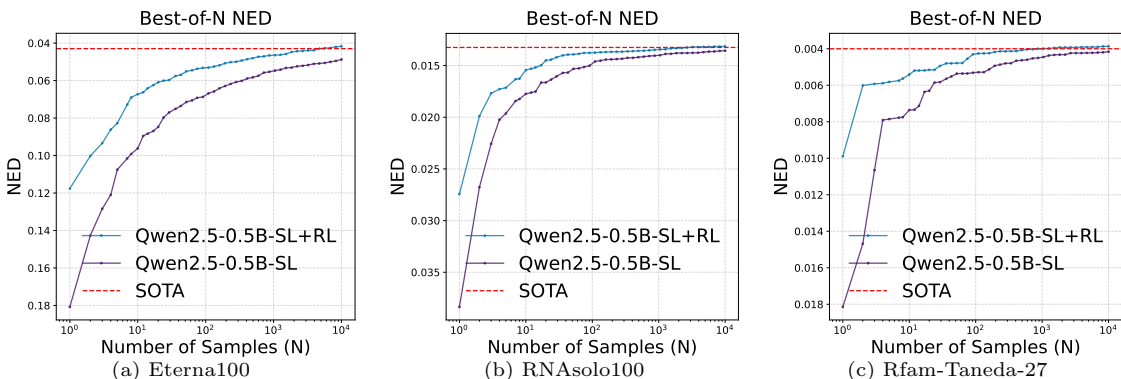


Fig. S2. Best-of- N curves for SL and SL+RL models in terms of Normalized Ensemble Defect (NED) on three data sets. See Fig. 7 in the main text for the corresponding Best-of- N curves on Boltzmann probability.

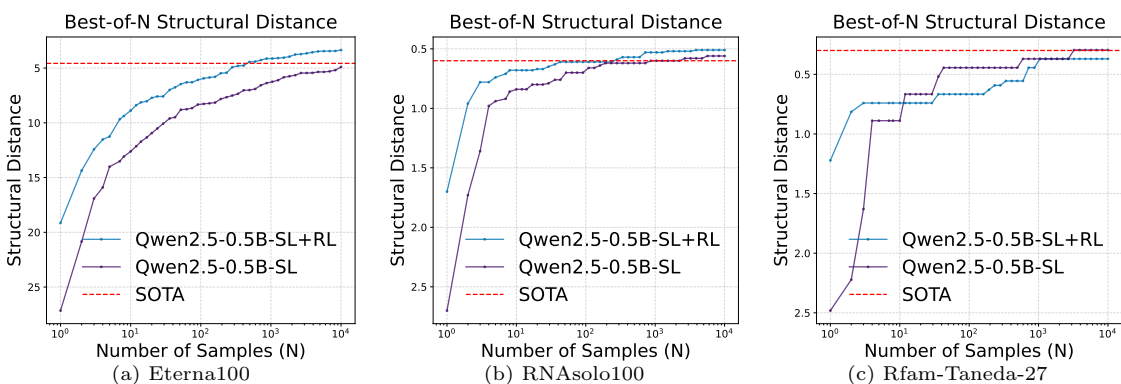


Fig. S3. Best-of- N curves for SL and SL+RL models in terms of Structural Distance on three data sets. See Fig. 7 in the main text for the corresponding Best-of- N curves on Boltzmann probability.

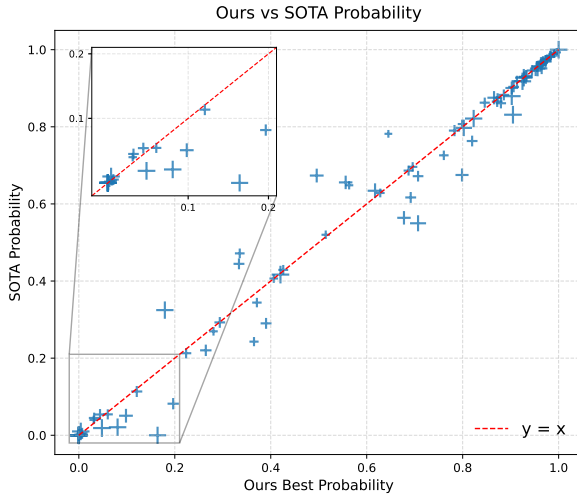


Fig. S4. X-Y plot of Boltzmann probability comparing SAMFEO and Ours (SL+RL) model on the Eternal100 test set. Our advantage is most salient on long and hard-to-design puzzles.

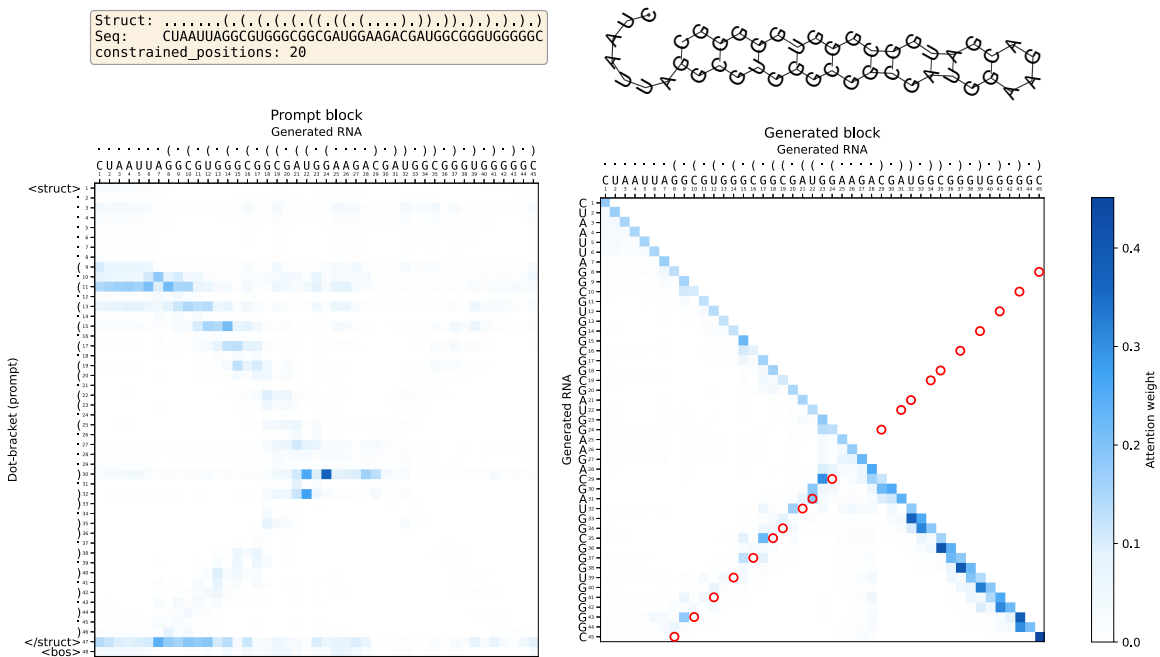


Fig. S5. For puzzle #33 of the Eterna100 test set, the figure visualizes causal self-attention in our decoding. The attention weights shown are averaged over all heads of the last self-attention layer. The left panel shows attention between the prompt (dot-bracket structure) and generated RNA tokens, while the right panel shows attention among generated RNA tokens. The target structure (dot-bracket) and generated RNA sequence appear at the top left, and the corresponding secondary structure is shown at the top right; red circles mark constrained base-pair positions.

Method	# of MFE/uMFE (\uparrow)	
	Eterna100	Rfam-Taneda-27
Eastman <i>et al.</i> ((Eastman <i>et al.</i>, 2018))	60 / 42	– / –
LEARNA ((Runge <i>et al.</i>, 2019))	67 / –	23 / –
Meta-LEARNA ((Runge <i>et al.</i>, 2019))	68 / –	24 / –
Ours (SL+RL)	75 / 73	24 / 24

Table S1. Comparison of RL methods on Eterna100 and Rfam-Taneda-27. The baselines' numbers are taken from those papers and they only reported MFE metrics. Our work substantially outperforms them on Eterna100.